Journal of Magnetic Resonance 210 (2011) 69–74

Contents lists available at ScienceDirect

Journal of Magnetic Resonance

journal homepage: www.elsevier.com/locate/jmr

Low-frequency NMR with a non-resonant circuit

Timothy Hopper [a], Soumyajit Mandal [a], David Cory [a,b], Martin Hürlimann [a], Yi-Qiao Song [a,*]

[a] Schlumberger-Doll Research, Cambridge, MA 02169, USA
[b] University of Waterloo, Waterloo, Canada

ARTICLE INFO

Article history:
Received 22 December 2010
Revised 11 February 2011
Available online 17 February 2011

Keywords:
Non-resonant NMR
Non-resonant transmitter
Switching transmitter
Digitally-tuned receiver
Well-logging

ABSTRACT

Nuclear magnetic resonance typically utilizes a tuned resonance circuit with impedance matching to transmit power and receive signal. The efficiency of such a tuned coil is often described in terms of the coil quality factor, *Q*. However, in field experiments such as in well-logging, the circuit *Q* can vary dramatically throughout the depth of the wellbore due to temperature or fluid salinity variations. Such variance can result in erroneous setting of NMR circuit parameters (tuning and matching) and subsequent errors in measurements. This paper investigates the use of a non-resonant transmitter to reduce the circuit sensitivity on *Q* and demonstrates that such circuits can be efficient in delivering power and current to the coil. We also describe a tuned receiver circuit whose resonant frequency can be controlled digitally. Experimental results show that a range of common NMR experiments can be performed with our circuits.

1. Introduction

Nuclear magnetic resonance (NMR) has been used for decades with a coil and capacitors forming a resonant circuit for both transmission and reception. The external properties of such a circuit are well characterized by three parameters: the resonance frequency, the characteristic impedance and the quality factor. The circuit is impedance-matched to an RF power amplifier (typically 50 Ω) for efficient power transmission to the coil during excitation. In field experiments such as well-logging, the instrument experiences large changes of temperature, significantly affecting the *Q* of the coil. In addition, the presence of highly-conductive saline water in the rock formations can induce eddy currents that drastically lower *Q*. Such a change in *Q* can significantly impact the accuracy of the measurement results. This paper proposes the use of a non-resonant transmitter to reduce the circuit sensitivity to temperature and salinity changes.

The term "non-resonant NMR" has been used in a variety of papers, but in somewhat different contexts. For instance, Murphee et al. constructed a tuning free, ultra-broadband probe for NMR that essentially consists of a transmission line [1] from DC-300 MHz. Previous work on transmission line-like probes by Lowe, Whitson, Kubo, Ichikawa and Engelsberg used a finite number of cascaded LC circuit sections [2–4]. Other NMR studies that used the term "non-resonant" involved manipulating the spins by suddenly switching the direction of the static magnetic field [5,6]. The formation of echoes has been demonstrated using sudden field reversal [7] and multiple echoes using compensated pulse sequences [8]. In this paper we use the term to mean the use of transmitter or receiver circuits with natural oscillation frequencies that are substantially different from the Larmor frequency.

This paper discusses the design and operation of a non-resonant circuit for spin excitation made solely with RF switches and no tuning or matching capacitors. We show that at low frequency and with low-inductance coils, such non-resonant circuits can achieve efficient power transmission and adequate current to use for RF excitation. We describe in detail the operation of the non-resonant circuit, its electronic implementation and experimental NMR results.

2. Non-resonant circuit for NMR

The block diagram for the overall NMR system is shown in Fig. 1. It consists of four main parts: the non-resonant transmitter, a tunable resonant receiver or probe, a data acquisition system based on National Instruments Data Acquisition card (NI-DAQ), and software running on a personal computer (PC). We denote the inductance of the transmit coil and its quality factor at the Larmor frequency ω_0 by L_1 and Q_1, respectively. The performance of a general transmitter is well characterized by two measures, namely *power transfer efficiency* and *amount of delivered current*. The power transfer efficiency is defined as the ratio of output power delivered to input power consumed. In a non-impedance-matched transmitter, such as our non-resonant design, this quantity approaches 100% when the source resistance is much smaller than the load resistance. Specifically, we can use a voltage source with low output impedance, such as a large battery, and switches with

* Corresponding author. Address: 1 Hampshire St., Cambridge, MA 02169, USA. Fax: +1 617 768 2386.
E-mail address: ysong@slb.com (Y.-Q. Song).

1090-7807/$ - see front matter © 2011 Elsevier Inc. All rights reserved.
doi:10.1016/j.jmr.2011.02.014

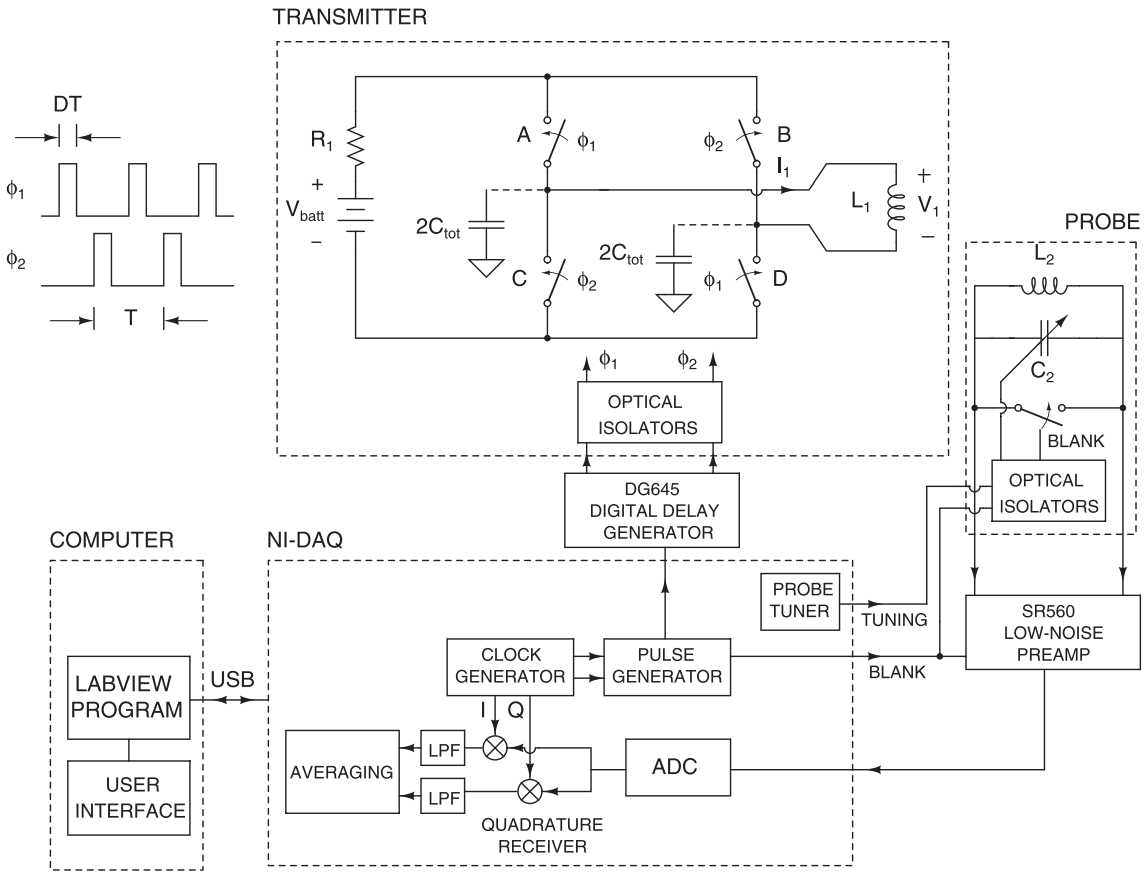

Fig. 1. Block diagram of the entire NMR spectrometer. The figure includes a simplified schematic of the H-bridge transmitter with the coil attached and control waveforms for the switches.

low on-resistance to make our non-resonant transmitter highly efficient. However, an impedance-matched transmitter is, by definition, limited to an efficiency of 50%. In practice such transmitters have even lower efficiencies since they are constructed with linear power amplifiers. Thus we can significantly increase transmitter efficiency by removing the impedance-matching constraint. Impedance-matched systems have the advantage of reduced reflections from cables and connectors. However, these benefits are insignificant at low frequencies since the relevant wavelength is much larger than the sizes of the electronic components.

Our transmitter circuit does not contain any tuning or matching capacitors. The simplest way to analyze it is to assume that the spins act as a band-pass filter with very high quality factor. Because of this frequency-selective behavior, only the fundamental frequency component of the coil current will be of interest for the spin dynamics. As a result we can define all passive circuit components in the transmitter in terms of their impedances at ω_0 and analyze it in steady state using the standard tools of linear AC circuit theory. In order to calculate the sinusoidal current amplitude $I(\omega_0)$ delivered to the transmitter coil L_1 let us assume that the transmitter outputs square voltage pulses with amplitude V_{RF} and duty cycle D, where $0 \leqslant D \leqslant 1$. We then find that

$$I(\omega_0) \approx \left(\frac{4V_{batt}}{\pi}\right)\frac{\sin(\pi D)}{Z_L}. \quad (1)$$

Here $Z_L = \omega_0 L_1$ is the impedance of the coil at ω_0. Thus non-resonant transmitters can efficiently deliver large amounts of current into small coils at low frequencies. For example, consider a solenoid of diameter 2 cm, length 3 mm, and five turns wound with AWG 24 copper wire (0.5 mm diameter). The low-frequency inductance of this coil will be approximately 820 nH, resulting in $Z_L = 1.5\ \Omega$ at 300 kHz. The output power of the transmitter depends on the duty cycle, as in class-D audio amplifiers, and is maximized when $D = 0.5$.

The RF voltage V_{RF} is ultimately generated from a DC voltage source V_{batt}, which may be a battery, rectifier, linear regulator, or switching regulator. In a traditional transmitter the value of V_{batt} has no relationship to V_{RF}, but in our non-resonant transmitter the two quantities are equal.

We assume that the Q of our coil is much greater than 1 even in the worst case, i.e., in very saline media at very high temperatures. As a result, the impedance of our non-resonant circuit will always be dominated by the inductor, i.e., approximately equal to Z_L. The inductance of a coil is a much weaker function of temperature and salinity than its resistance and Q. Thus our non-resonant transmitter will be more robust to changes in these parameters than a resonant transmitter. In order to make the complete NMR system insensitive to these parameters the receiver should also be non-resonant. Such receivers are the focus of current research in our laboratory.

3. Transmitter circuit analysis

Our basic non-resonant transmitter design consists of a set of four MOSFET RF switches (labeled A, B, C and D), arranged in a circuit known as an H-bridge, as shown in Fig. 1. The switches are controlled by two non-overlapping digital signals denoted as ϕ_1 and ϕ_2. The signals ϕ_1 and ϕ_2 are used to drive the two sets of switches, AD and BC, such that the voltage source V_{batt} is connected with alternating polarity across the coil and an oscillatory coil

current is created. A load resistor R_1 is used in series with the batteries in order to limit the current into the MOSFETs. The value of R_1 was set to a value that was low enough to ensure high transmitter efficiency, but high enough to prevent damage to the switches in case A and C (or B and D) were turned on simultaneously. The need for this resistor can be eliminated by using an intelligent bridge-driver circuit that automatically imposes a non-zero "dead time" between the two clock phases, making such "shoot-through" events impossible. Several suitable integrated circuits have been developed for the automotive market and are commercially available. Finally, L_1 is the inductance of the excitation coil, and C_{tot} is the parasitic output capacitance of each MOSFET switch.

To first order, we may assume that the switches are ideal, and that there are no stray capacitances. In this case the current through the coil is given by

$$I_1 = \pm\frac{V_{batt}}{R_1}(1 - e^{-t/\tau_1}). \tag{2}$$

Here we have assumed $I_1(0) = 0$ and defined the time constant $\tau_1 \equiv L_1/R_1$. The signs correspond to the positive and negative phases, respectively. At Larmor frequencies that are high enough for the condition $t \ll \tau_1$ to be always valid, i.e., when $1/f_0 \ll \tau_1$, the expression above can be linearized to

$$I_1 = \pm\frac{V_{batt}}{R_1}\left(\frac{t}{\tau_1}\right) = \pm\left(\frac{V_{batt}}{L_1}\right)t. \tag{3}$$

We see that in this regime the current in the transmit coil is independent of the value of the series resistor R_1. In the real circuit the situation is complicated by the presence of capacitors. A more detailed model of each switch is shown in Fig. 2. In addition to inevitable stray capacitance, each switch is associated with intentional capacitance within the snubber circuit formed by *D*, R_d, and C_d. This dissipative circuit acts as a voltage clamp. It prevents the formation of large inductive voltage spikes ($V_1 = L_1\frac{dI_1}{dt}$) that can damage the switches. By limiting the value of $|dI_1/dt|$ the circuit forces I_1 to grow (or decay) gradually instead of suddenly turning on (or off).

After all the switches and snubber circuits turn off, the total parasitic capacitance, denoted by C_{tot}, is discharged by the remaining current in the inductor. A series resonant circuit is then formed by L_1, C_{tot}, and their associated losses (resistances). Thus we expect I_1 to ring down to zero after the pulse in an oscillatory fashion, with the natural oscillation frequency being given by

$$f_1 = \frac{1}{2\pi\sqrt{L_1 C_{tot}}}. \tag{4}$$

The problem of delivering current to an NMR coil is similar in many ways to that of energizing motor windings and loudspeakers, which also behave as inductors. It is therefore significant that variants of the H-bridge (or class-D) circuit shown in Fig. 1 are commonly used in high-efficiency motor drivers and audio amplifiers [9]. The switches used on the H-bridge transmitter need to be able to conduct high current and voltage whilst their switching speed has to be high enough to excite the spins at our resonance frequency. The commercial availability of fast, high-power MOSFET switches and switch drivers (e.g., from Behlke GmbH, www.behlke.de) enables the H-bridge and similar switching circuits to deliver several Amperes of current at frequencies up to a few MHz. In addition, single-chip versions using integrated switches can be used for low-power applications, such as microcoil NMR, at even higher frequencies [10].

4. Overall system design

The entire experimental apparatus was controlled using a National Instruments NI-DAQ that uses the DAQmx application programming interface (API). The DAQ was controlled from LabVIEW software running on a standard PC. The control signals for all switches on the probe, pre-amplifier and tunable receiver bank were routed from the NI-DAQ as shown in Fig. 1.

The non-resonant H-bridge transmitter was built using prototype S-HTS 11–14 MOSFET switches from Behlke GmbH and implemented on a copper-clad circuit board. Behlke builds a series of such HTS MOSFET switches. HTS switches are made up of a large number of MOSFETs, both in parallel and in series. They are combined into a compact, low-inductance switching bank. The switches are controlled via their gates, instead of being operated in breakdown mode like avalanche transistor switches. The use of the gates gives rise to a high degree of reliability and fast-switching performance. TTL-compatible logic lines are used to control the switches on the input side. These logic lines feed into a special internal driving circuit that is used to drive the MOSFETs synchronously and with low impedance. This circuit uses a voltage up-converter to transform logic-level control signals into the high gate voltages necessary to turn on the MOSFETs. It also takes care of signal conditioning, auxiliary voltage monitoring, frequency limiting, and temperature protection. A summary of the properties of the switches was provided by Behlke, and is shown in Table 1.

The single-phase output from the NI-DAQ is fed into a digital delay generator (DG645, Stanford Research Systems) in order to produce the two non-overlapping phases ϕ_1 and ϕ_2 (see Fig. 1) necessary to drive the H-bridge. The output of the delay generator is fed into the H-bridge through a set of optical isolators (HCPL-2201, Avago) in order to reduce noise by isolating the ground voltages of the transmitter and DAQ and thus removing a pickup-prone ground loop.

The NMR signal is detected by a separate coil that is connected to a tuned circuit but without the usual impedance-matching capacitor [10,11]. Specifically, the receiver coil L_2 is tuned by a capacitor C_2 to create a parallel LC circuit whose resonance frequency can be digitally controlled as shown in Fig. 3. The resonant frequency is varied by MOSFET switches that control a binary-weighted bank of four mica capacitors present within C_2 and is given by

$$f_{res} = \frac{1}{2\pi\sqrt{L_2 C_2}}, \qquad C_2 = C_{fixed} + BC_0, \quad 0 \leqslant B \leqslant 15. \tag{5}$$

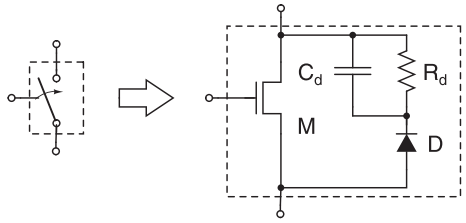

Fig. 2. Equivalent circuit of each switch within the transmitter.

Table 1
Summary of Behlke MOSFET switch characteristics. Source: Behlke S-HTS 11–14 preliminary data sheet.

Parameter	Value
Peak operating voltage	1200 V
Peak current	140 A
On resistance	<0.6 Ω
Turn-on delay time	<100 ns
Switch recovery time	<300 ns

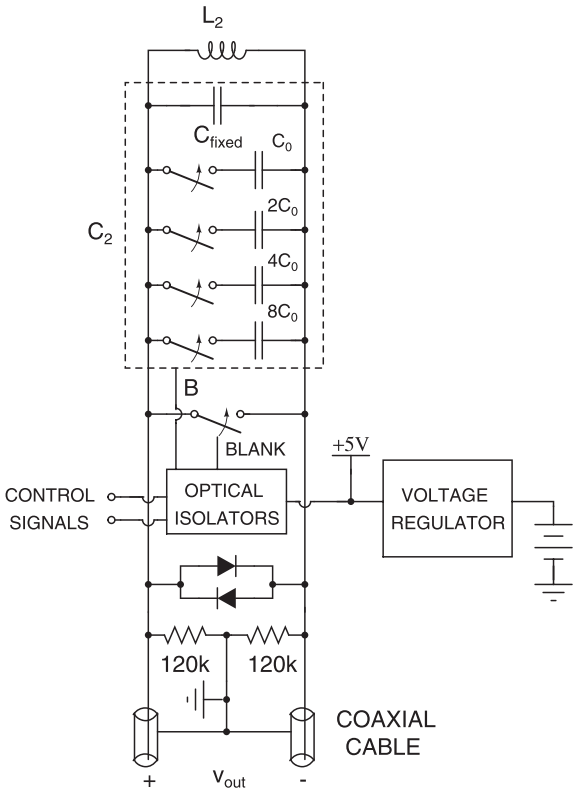

Fig. 3. Schematic of the tunable receiver network showing the fixed capacitor C_{fixed} and the 4-bit switchable capacitor bank.

Here B is the decimal representation of the 4-bit binary vector that controls the state of the switches (0 = OFF, 1 = ON). Since the receiver circuit does not have to handle large signals integrated transistors can be used as switches instead of the PIN diodes commonly used to build frequency-switchable NMR coils [12]. We therefore used MOS switches with a low on-resistance of $R_{on} = 0.3\ \Omega$ (ADG801, Analog Devices). The quality factor of the tuned receiver circuit is given by

$$\frac{1}{Q_2} = \frac{1}{Q_L}\left[1 + \frac{(R_{on}/R_s)}{1 + C_{fixed}/(BC_0)}\right]. \tag{6}$$

Here R_s and Q_L are the series resistance and quality factor of the receiver coil. Eq. (4) shows that increasing the frequency tuning range by decreasing the ratio C_{fixed}/C_0 lowers the value of Q_2. In our case $C_{fixed} = 7.4$ nF, $C_0 = 0.5$ nF, and $R_s \approx 1.0\ \Omega$, so the switches degrade the quality factor by a maximum of 15%. At resonance the impedance of the probe is resistive, and is given by $R_{probe} \approx \omega_{res} L_2 Q_2$.

The NMR voltage developed across the LC circuit is sensed differentially by a low-noise pre-amplifier that has a high input-impedance (SR-560, Stanford Research Systems). Differential sensing renders the system largely immune to common-mode electrostatic (capacitive) pickup, which is often an important issue with high-impedance probes at low operating frequencies.

The noise figure of the receiver is defined as the ratio of input SNR to output SNR. In general, minimum noise figure is obtained when the source resistance, i.e., the impedance of the tuned probe at resonance, is equal to $R_n = \sqrt{e_n^2}/\sqrt{i_n^2}$, where e_n^2 and i_n^2 are the power spectral densities of the input-referred voltage and current noise of the pre-amplifier. This condition is known as noise matching. However, at our low operating frequency current noise is negligible for FET-input pre-amplifiers such as the SR-560. As a result, resonating the coil maximizes the amount of passive and noiseless voltage gain before the pre-amplifier and minimizes noise figure. In addition, our operating frequency was low enough for reflections from 50 Ω cables and connectors to be negligible. We therefore used a tuned LC circuit as the probe, and made no attempt to match its impedance to 50 Ω. At resonance the noise figure is given by

$$NF = 10\ \log_{10}\left(\frac{R_{preamp} + R_{probe}}{R_{probe}}\right) = 10\ \log_{10}\left(1 + \frac{R_{preamp}}{R_{probe}}\right). \tag{7}$$

Here R_{preamp} is the input-referred noise resistance of the pre-amplifier. Thus the noise figure decreases as R_{probe} increases. We have $R_{probe} = 3.2$ kΩ at a Larmor frequency of 290 kHz and $R_{preamp} = 1.0$ kΩ at 300 K, resulting in an excellent receiver noise figure of 1.1 dB at resonance.

The output of the pre-amplifier is digitized by the 16-bit analog-to-digital converter (ADC) present within the NI-DAQ at four times the Larmor frequency. The acquisition clock is only enabled during acquisition windows that have user-defined widths and are centered on expected echo locations.

In addition to the pulse generator, the NI-DAQ also contains a complete digital quadrature receiver written in the LabVIEW graphical programming language. The receiver down-converts the acquired signal into real and imaginary (I and Q) channels. It then transfers the results to a graphical user interface (GUI), also written in LabVIEW. The GUI allows the user to set pulse sequence parameters, tune the receiver, view outputs, perform further signal processing and in general control the system much like a modern NMR spectrometer.

5. Experimental results

We used an "inside out" NMR geometry based on the Jasper Jackson design [13]. This design uses two axially-polarized cylindrical permanent magnets separated from each other by a fixed distance d. The value of d can be varied to change properties of the magnetic field. Specifically, the field strength and gradient at a given depth of investigation (DOI, i.e., radial distance outward from the surface of the magnet) decrease with d. Our magnet design resulted in a Larmor frequency of $f_0 = 275$ kHz and a field gradient of $g = 12.8$ kHz/cm at a DOI of 9.0 cm.

We chose to use a separate receive coil, with transmit and receive coils placed orthogonal to each other to provide approximately 20 dB of isolation. Both coils were circular solenoids with properties that are shown in Table 2. The sample was cylindrical in shape. It was aligned and centered within the transmit coil, while the receive coil was located on one side (6.25 cm from the center of the sample).

The coil current waveform was analytically calculated and used as an input to a spin dynamics model implemented in Mathematica™. The model was used to calculate the energy required to tip the spins into the transverse plane, given the current waveform in the coil. These analytical results were confirmed against nonlinear time-domain simulations of the circuit using SPICE, a popular general-purpose circuit simulator. We connected seven lead-acid car batteries in series to create the DC voltage source shown in Fig. 1. Each battery provides a nominal output voltage of 12.6 V, resulting in $V_{batt} = 88$ V. In addition, we assumed $f_0 = 290$ kHz,

Table 2
Properties of the transmit coil, receive coil, and sample used in our experiments.

Name	Radius	Turns	Inductance	Q (275 kHz)
Transmit coil	5.75 cm	8	10.6 μH	25
Receive coil	4.5 cm	12	32 μH	57
Sample	3.75 cm	–	–	–

$R_1 = 5.2\ \Omega$, $L_1 = 10.6\ \mu H$, and $D = 0.38$. The simulated natural circuit oscillation frequency was $f_1 \approx 1.7$ MHz, corresponding to $C_{tot} \approx 830$ pF. The simulated peak current was 6.4 A, and the length of a 90° pulse was seven periods of the Larmor frequency, corresponding to $\gamma B_1/(2\pi) = 10.4$ kHz.

Fig. 4 shows the measured transmitter current I_1 during a 180° pulse. The measured coil current is very close to the simulated current. The "glitches" visible within each excitation period coincide with switches turning on or off, which result in inductive voltage spikes that are suppressed by the snubber circuits. Oscillations during the ring down period occur at the natural oscillation frequency f_1 of the transmitter (approximately 1.7 MHz), and not at the Larmor frequency. As a result, the effects of pulse ring down on spin dynamics are negligible.

Experimentally, we were able to digitally control the resonant frequency of the receiver between 230 kHz ($B = 15$) and 320 kHz ($B = 0$). The quality factor increased from 50 to 60 as the resonant frequency was varied over this range. Both these results are close to theoretical calculations.

We conducted various NMR experiments on doped water, tap water, and vegetable oil samples. A nutation experiment was conducted to find the optimal length of the 90° and 180° pulses (T_{90} and T_{180}, respectively). In this experiment we used a CPMG sequence where T_{180} was fixed at 14 RF cycles (corresponding to $\gamma B_1/(2\pi) = 10.4$ kHz) and T_{90} was varied. The second echo was integrated and is shown as circles in Fig. 5. The smooth curves also shown on the plot are defined as

$$F_{ideal}(T_{90}) = \sin(\gamma B_1 T_{90}),$$
$$F_{fit}(T_{90}) = \frac{\int_{1-\delta}^{1+\delta} \sin(\gamma B_1 T_{90} x)dx}{\int_{1-\delta}^{1+\delta} \sin(\frac{\pi}{2}x)dx} = F_{ideal}(T_{90})\left[\frac{\mathrm{sinc}(\gamma B_1 T_{90}\delta)}{\mathrm{sinc}(\frac{\pi}{2}\delta)}\right]. \quad (8)$$

The function $F_{ideal}(T_{90})$ is the ideal sinusoidal nutation curve expected for a homogenous B_1 field, while $F_{fit}(T_{90})$ is a fit to the data that corrects for the effects of T_{90} pulse bandwidth in inhomogeneous fields. The parameter δ accounts for variations in nutation angle within the excited volume. We obtained a good fit to the measured data for $\delta = 0.35$. This much RF inhomogeneity is not unreasonable, given that the receiver coil is located along one edge of the excited volume.

The CPMG echo train obtained from an oil sample after $N = 500$ averages is shown in Fig. 6. Each echo has been individually low-pass filtered with a sixth-order Butterworth low-pass filter with a bandwidth of 6 kHz, and a simple two-part phase cycle has been used to cancel DC offsets and RF ringing from the signal. Fig. 6 also shows the detailed shape of the second echo, which has an SNR of approximately 25. This result agrees very well with the theoretically calculated SNR. The bandwidth of the excited signal is approximately $\pm\gamma B_1/(2\pi) = \pm 10.4$ kHz. This value is considerably larger than the detection bandwidth, which is set by the probe to

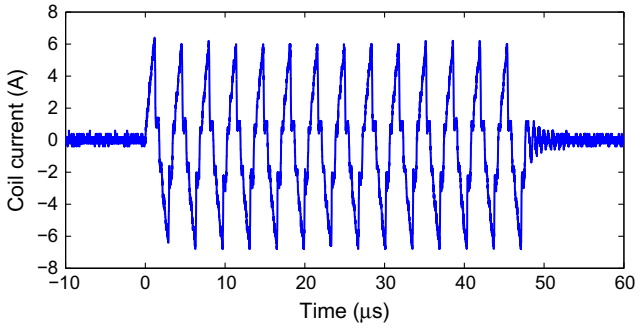

Fig. 4. Measured current through the transmitter coil L_1 during a 180° pulse for a duty cycle of 38%.

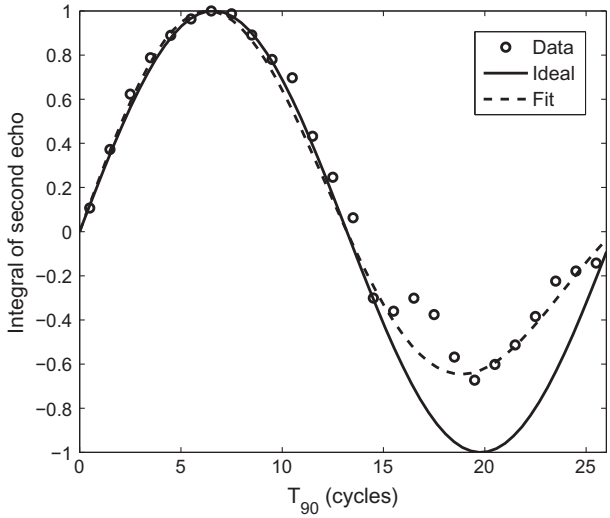

Fig. 5. Nutation experiment at 290 kHz. The length of the T_{90} pulse was varied, while the T_{180} pulse length was fixed to 14 RF cycles.

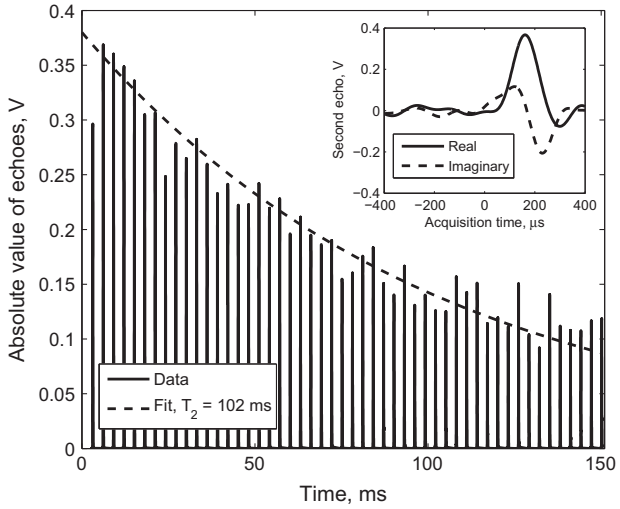

Fig. 6. CPMG echo train with $T_E = 3$ ms measured from an oil sample after $N = 500$ averages. The half-power spectral width of each echo is approximately 4.5 kHz. This corresponds well with the expected width, i.e., the probe bandwidth of 4.8 kHz. Inset: The real and imaginary components of the second echo.

±2.4 kHz. Only a fraction of the excited signal is detected in this "super-Q" regime, resulting in signal distortion [14]. The detection bandwidth can be increased without affecting SNR by adding feedback around the pre-amplifier [15,16]. Alternatively, the transmitter battery voltage, which is approximately proportional to B_1, can be considerably reduced without affecting SNR.

6. Discussion

We have demonstrated the design and operation of an NMR system based on a non-resonant transmitter circuit. Experimental results with CPMG and other sequences show that the system is capable of carrying out relaxation and diffusion measurements similar to other relevant NMR systems.

The use of a non-resonant transmitting coil is likely to provide new degrees of flexibility in NMR system design in addition to insensitivity to coil Q changes. For example, being a broadband system, non-resonant NMR allows the NMR frequency to be changed

purely through software, i.e., without tuning. For NMR systems in which the magnetic field is changing as a function of depth, our system enables us to change the operation frequency without the need for adjusting tuning and matching capacitors. This aspect can be significant for high-power NMR systems where adjustable tuning systems are often constructed using slow and unreliable mechanical relays as switches.

This paper demonstrates a non-resonant transmitter that is suitable for low-frequency NMR. Non-resonant transmitter circuits can deliver large amounts of current to NMR coils when their impedance Z_L is low, as shown in (1). Thus this concept may also be useful in the case of microcoil NMR where the inductance of the small coil can be extremely low. For example, consider a solenoid of diameter 1 mm, length 3 mm, and five turns wound with copper wire (0.1 mm diameter). The low-frequency inductance of this coil will be approximately 23.5 nH, resulting in $Z_L = 4.4\ \Omega$ at 30 MHz.

This paper also demonstrates a resonant receiver circuit that does not need a matching capacitor. It was used to construct a receiver with very low noise figure from off-the-shelf parts. In addition, we showed that the resonant frequency of the receiver can be digitally set by using electronic switches to control a bank of capacitors without degrading its noise figure. Moving to a completely non-resonant transmit and receive system is the focus of on-going research in our laboratory.

7. Conclusions

We demonstrate an unconventional NMR circuit that can deliver good power transmission efficiency and RF power for spin excitation. Such system is made possible by the recent commercial availability of fast-switching, high-power MOSFETs and drivers. We present a full NMR system based on this non-resonant circuit. This concept opens up new flexibilities in NMR system design, in particular for low-frequency NMR and microcoil NMR.

References

[1] D. Murphee et al., An easily constructed, tuning free, ultra-broadband probe for NMR, J. Magn. Reson. 188 (1) (2007) 160–167.
[2] I.J. Lowe, M. Engelsberg, A fast recovery pulsed nuclear magnetic resonance sample probe using a delay line, Rev. Sci. Instrum. 45 (5) (1974) 631–639.
[3] I.J. Lowe, D.W. Whitson, Homogeneous RF field delay line probe for pulsed nuclear magnetic resonance, Rev. Sci. Instrum. 48 (3) (1977) 268–274.
[4] A. Kubo, S. Ichikawa, Ultra-broadband NMR probe: numerical and experimental study of transmission line NMR probe, J. Magn. Reson. 162 (2) (2003) 284–299.
[5] M. Packard, R. Varian, Free nuclear induction in the earth's magnetic field, Phys. Rev. 93 (1954).
[6] A. Abragam, Principles of Nuclear Magnetism, first ed., Clarendon, Oxford, UK, 1978.
[7] R. McDermott et al., Liquid-state NMR and scalar couplings in microtesla magnetic fields, Science 295 (5563) (2002) 2247–2249.
[8] T. Brill et al., Nonresonant multiple spin echoes, Science 297 (5580) (2002) 369–372.
[9] J.G. Kassakian, M.F. Schlecht, G.C. Verghese, Principles of Power Electronics, first ed., Prentice Hall, 1991.
[10] N. Sun et al., CMOS RF biosensor utilizing nuclear magnetic resonance, IEEE J. Solid-State Circ. 44 (5) (2009) 1629–1643.
[11] K.W. Gray, W.N. Hardy, J.D. Noble, Optimized pulsed NMR single coil circuit design, Rev. Sci. Instrum. 37 (5) (1966) 587–588.
[12] C.-H. Choi, J.M.S. Hutchison, D.J. Lurie, Design and construction of an actively frequency-switchable RF coil for field-dependent magnetisation transfer contrast MRI with fast field-cycling, J. Magn. Reson. 207 (1) (2010) 134–139.
[13] R.K. Cooper, J.A. Jackson, Remote (inside-out) NMR. I: remote production of region of homogeneous magnetic field, J. Magn. Reson. 41 (3) (1980) 400–405.
[14] B.H. Suits, A.N. Garroway, J.B. Miller, Super-Q detection of transient magnetic resonance signals, J. Magn. Reson. 132 (1) (1998) 54–64.
[15] D.I. Hoult, Fast recovery, high sensitivity NMR probe and preamplifier for low frequencies, Rev. Sci. Instrum. 50 (2) (1979) 193–200.
[16] D.I. Hoult, Fast recovery with a conventional probe, J. Magn. Reson. 57 (3) (1984) 394–403.